REVISTA DE LA
ASOCIACIÓN GEOLÓGICA
ARGENTINA
www.geologica.org.ar
Diciembre 2024

U-Th-Pb chemical dating in monazite in the andalusite-garnet-staurolite-sillimanite schists of the Cushamen Complex (Chubut, Argentina): reconstructing the P-T-t path

Samanta SERRA-VARELA[1,2], Sebastián O. VERDECCHIA[3,4], Fernando COLOMBO[3,4], Carlos I. LEMBO WUEST[3,4], Manuela E. BENÍTEZ[3,4], Juan A. MURRA[3] and Edgardo G. BALDO[3,4]

[1]Consejo Nacional de Investigaciones Científicas y Técnicas (CONICET) Instituto de Investigación en Paleobiología y Geología (IIPG), Gral. Roca 1242, Gral. Roca, Argentina.

[2]Universidad Nacional de Río Negro. Sede Alto Valle y Valle Medio (UNRN). Instituto de Investigación en Paleobiología y Geología, Gral. Roca, Argentina.

[3]Universidad Nacional de Córdoba. Facultad de Ciencias Exactas, Físicas y Naturales. CICTERRA (CONICET-UNC). Av. Vélez Sarsfield 1611, Córdoba, Argentina.

[4]Consejo Nacional de Investigaciones Científicas y Técnicas (CONICET). Centro de investigaciones en Ciencias de la Tierra (CICTERRA). Av. Vélez Sarsfield 1611, Córdoba, Argentina.

E-mail: ssvarela@unrn.edu.ar

Editor: Ricardo A. Astini

Recibido: 26/12/2024

Aceptado: 19/03/2025

ABSTRACT

This study presents the first U-Th-Pb CHIME monazite dating in andalusite-garnet-staurolite-sillimanite schists from the Cushamen Complex (Chubut, Argentina). It represents the first age obtained by this method in Argentina. X-ray elemental distribution maps were performed to assess possible zoning patterns resulting in zoned monazites with Th depletion and Ce enrichment toward the rims. Results reveal a correlation between the polymetamorphic P-T evolution with three groups of ages calculated from punctual analyses of monazite with ages of ca. 354, 333 and 300 Ma, consistent with main metamorphic events identified regionally in North Patagonia.

Keywords: petrochronology, polymetamorphism, Paleozoic basement, U-Th-Pb CHIME

RESUMEN

Datación química U-Th-Pb en monacita en los esquistos con andalusita-granate-estaurolita-sillimanita del Complejo Cushamen (Chubut, Argentina): implicancias en la reconstrucción de la trayectoria P-T-t.
Este estudio presenta la primera datación U-Th-Pb CHIME en monacitas de esquistos con andalucita-granate-estaurolita-sillimanita del Complejo Cushamen (Chubut, Argentina). La misma representa la primera edad obtenida con esta metodología en Argentina. Se realizaron mapas composicionales para evaluar posibles zonaciones en los cristales de monacita donde se observó una zonación con bordes empobrecidos en Th y ricos en Ce. Los resultados revelan una correlación entre la evolución polimetamórfica P-T y tres grupos de edades calculados a partir de análisis puntuales de monacita, con edades de ca. 354, 333 y 300 Ma, consistentes con eventos metamórficos regionales en Patagonia Norte.

Palabras clave: petrocronología, polimetamorfismo, basamento paleozoico, U-Th-Pb CHIME

INTRODUCTION

One of the challenges in metamorphic petrology is determining the age of metamorphic events, whether in contexts involving a single metamorphic event or in polymetamorphic terrains (e.g., Engi et al. 2017). For this purpose, two main groups of methodologies are commonly employed, each with its own advantages and limitations. The first group includes methods that require the separation and concentration of the mineral to be dated, such as K-Ar and Ar-Ar for potassium-bearing phyllosilicate and amphibole, Sm-Nd and Lu-Hf for garnet, and U-Pb for zircon. The second group comprises in-situ measurement techniques, such as U-Pb in garnet and the U-Th-Pb chemical dating method (CHIME) in monazite. In-situ techniques are particularly valuable for studying metamorphism, especially within the petrochronology approach (e.g., Williams et al. 2017 and references therein). Petrochronology integrates temporal data with microstructural, mineralogical, and thermobarometric constrains, enabling the reconstruction of pressure – temperature – deformation - time (*P-T-D-t*) paths.

The CHIME method, or chemical dating of monazite (e.g., Suzuki and Kato 2008 and references therein), is widely used in the study of metamorphic rocks. This technique is relatively cost-effective compared to other methods and allows the determination of the age of metamorphic processes in different contexts. CHIME dating is conducted using an electron microprobe (EPMA) equipped with wavelength dispersive spectrometers (WDS), which enables the precise quantification of elemental concentrations in minerals.

In the present study, we report the first CHIME U-Th-Pb monazite dating results obtained using the electron microprobe at the Laboratorio de Análisis de Materiales por Espectrometría de Rayos X (LAMARX) of the Universidad Nacional de Córdoba (Argentina). This represents the first age obtained by this method in Argentina, marking a significant milestone for metamorphic petrology research in the country. This dating was carried out on a sample of andalusite-garnet-staurolite-sillimanite schist from the Cushamen Complex, previously studied by Serra-Varela et al. (2024). As a result, we constrained the proposed polymetamorphic P-T evolution to the upper Palaeozoic evolution of the North Patagonian Massif.

GEOLOGICAL SETTING

All over the North Patagonian Cordillera and its extra-Andean region two main middle to Upper Palaeozoic events can be recognized according to their metamorphic and deformational history. The oldest group would be related to a middle – late Devonian to early Carboniferous metamorphic event (Lucassen et al. 2004, Pankhurst et al. 2006, Martínez et al. 2012, Varela et al. 2015, Heredia et al. 2016, 2018, Hervé et al. 2018, Renda et al. 2021, Dicaro et al. 2023, Marcos et al. 2023, Rapela et al. 2024) whereas the younger occurred during the late Carboniferous – early Permian (Lucassen et al. 2004, Varela et al. 2005, Pankhurst et al. 2006, García-Sansegundo et al. 2009, Lopez de Luchi et al. 2010, Varela et al. 2015, Heredia et al. 2016, Oriolo et al. 2019, Marcos et al. 2020, Renda et al. 2021, Falco et al. 2022, Murra et al. 2022).

Moreover, the metasedimentary successions in these regions were linked to two main units: early to middle Palaeozoic Colohuincul and mid- to late Paleozoic Cushamen complexes (Serra-Varela et al. 2020 and references therein). The Cushamen Complex, initially defined as Cushamen Formation by Volkheimer (1964) and later renamed as Complex by Serra-Varela et al. (2020), is composed of low- to high-grade metasedimentary and metaigneous rocks (Dalla Salda et al. 1994, Cerredo 1997, Cerredo and López De Luchi 1998, Duhart et al. 2002, Giacosa et al. 2004). Near Cushamen town and Río Chico River (Chubut province), the Cushamen Complex is represented by low-grade rocks (phyllites, metapsammites and metaquartzites), schists, gneisses (e.g., Giacosa et al. 2004, Serra-Varela et al. 2024) and deformed Carboniferous granitoids (Pankhurst et al. 2006). A mid- to late-Paleozoic depositional age for the sedimentary protoliths of the Cushamen Complex was constrained through detrital zircon analyses, with maximum depositional ages of approximately 385 Ma and 369 Ma (Hervé et al. 2018, Marcos et al. 2020, respectively). Additionally, $^{87}Sr/^{86}Sr$ isotopic ratios in metacarbonates indicate a sedimentation age of approximately 385–335 Ma (Murra et al. 2022).

The andalusite-garnet-sillimanite-staurolite schist

The analyzed sample is a garnet-andalusite-staurolite-sillimanite schist from the Cushamen Complex (sample code MNP-2055; 42°08′32.5″ S –70°32′29.7″ W; Serra-Varela et al. 2024) obtained in the surroundings of Cushamen town, where this unit was originally defined (Fig. 1a). This schist is composed of andalusite pokiloblasts (chiastolite), staurolite, and garnet in a matrix of sillimanite (prismatic and fibrolite), biotite, muscovite, quartz, and plagioclase (Fig. 1b). As accessory minerals, the sample has rutile, ilmenite, apatite, monazite, zircon, magnetite, tourmaline and graphite. The main foliation is a S_2 crenulation foliation where S_1 is only

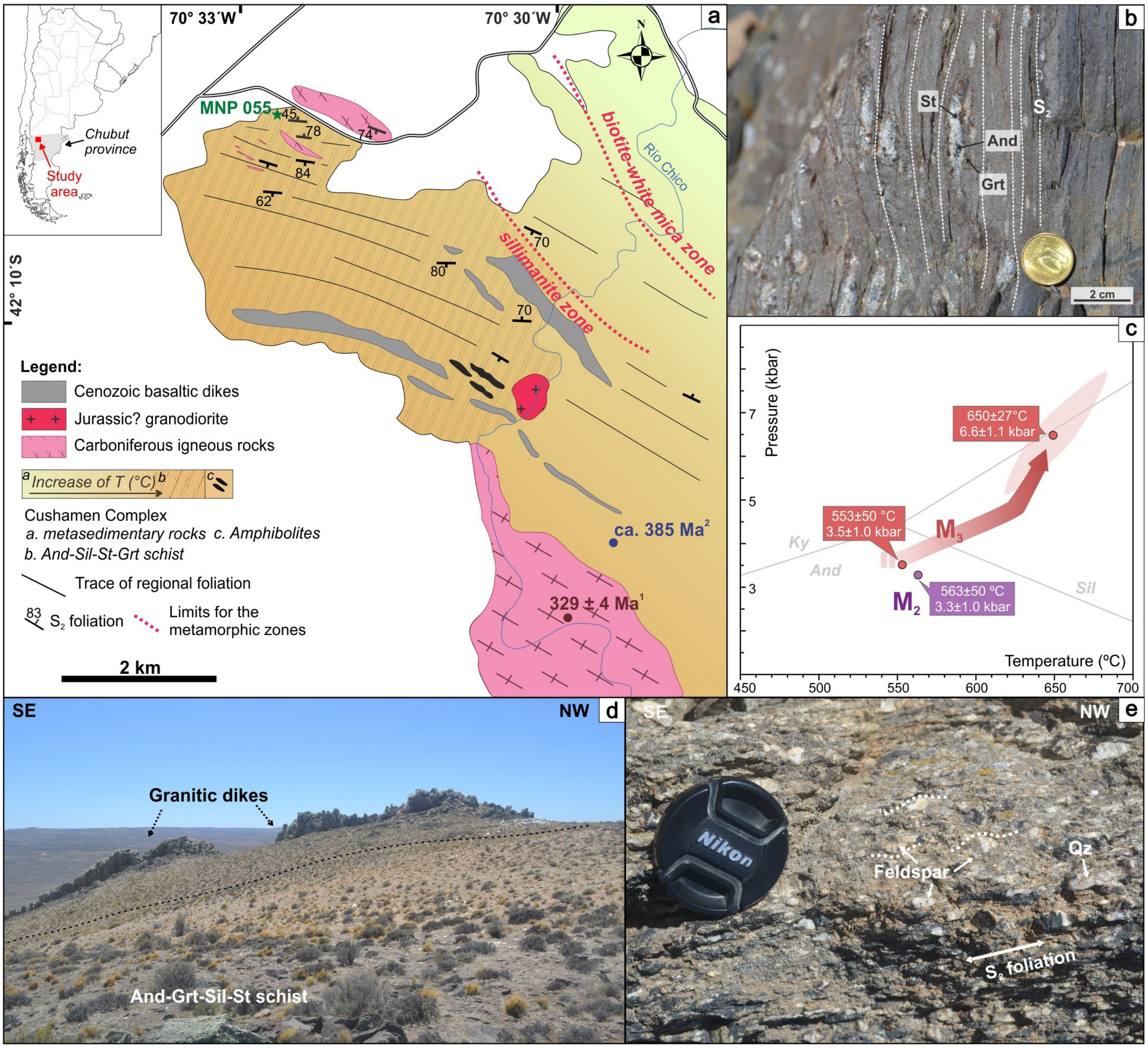

Figure 1. a. Simplified geological map of the studied area taken from Serra-Varela et al. (2024) showing the main lithostratigraphic units. Geochronological data from (1)Pankhurst et al. (2006) and (2)Hervé et al. (2018). b. Field photography of the andalusite – garnet – sillimanite – staurolite schist showing the penetrative S_2 foliation. c. Summary of *P–T* conditions calculated for M_2 and M_3 metamorphic events from Serra-Varela et al. (2024). d. Field photograph of the granitic dikes found intruding the metamorphic rocks from the area. e. Detail of the foliation found in the igneous rocks related to S_2 foliation of the metasedimentary sequence.

recognized in microlithons and deformation shadows around large andalusite porphyroblasts. Recently, Serra-Varela et al. (2024) proposed a polymetamorphic evolution for this unit represented by three metamorphic events, named M_1, M_2, and M_3. M_1 was synchronic to the development of the S_1 foliation and is defined by biotite (Bt_1) + muscovite (Ms_1) + quartz + plagioclase (mineral names are abbreviated cf. Whitney and Evans, 2010). Metamorphic conditions for this event could not be calculated since mineral compositions were re-equilibrated at higher metamorphic conditions. M_2 is defined by static growth of garnet (Grt_1) + andalusite reaching *P-T* conditions of ca. 3.3 kbar and ca. 563 °C based on isopleth thermobarometry from phase equilibria analyses (Fig. 1c). Grt_1 is defined as cores of large garnet porphyroblasts with higher contents of X_{Sps} and lower contents of X_{Alm} than its mantle and rim (Grt_{2-3}). Finally, M_3 event produces reabsorption of garnet (Grt_1) and new growth of garnet (Grt_{2-3}) in a mineral assemblage with sillimanite, staurolite, biotite (Bt_2), muscovite (Ms_2), plagioclase, and quartz. This stage of garnet growth is defined as the mantle and rim of large porphyroblasts as well as small porphyroblast with homogenous compositions SM_1 (de Suplementary Material). This event was synchronic with the development of a main penetrative S_2 foliation. Isopleth thermobarometry suggests *P-T* conditions from ca. 3.5 kbar and 553 °C to peak conditions of ca. 6.6 kbar and 650 °C (Fig. 1c).

In the western part of the study area, these schists are intruded by granitic stocks and dikes of NW–SE-trend (1–10 m wide, Fig. 1d). The intrusive bodies, composed of quartz, plagioclase, K-feldspar, biotite, and muscovite, exhibit a tectonic foliation (Fig. 1e) that is parallel to S_2 foliation in schists. For a more detailed description of the sample refer to Supplementary material S_1.

ANALYTICAL METHOD

In-situ mineral chemical analyses were conducted with a JEOL JXA-8230 Superprobe instrument at the Laboratory of Electron Microscopy and X-Ray Analysis (LAMARX) of Universidad Nacional de Córdoba (Argentina). To carry out the in-situ dating of monazites, the microprobe was calibrated following the recommendations of Vlach (2010). Full analytical details are listed in Table S_1, as Supplementary material.

RESULTS

Monazite morphology and microstructures

Monazite crystals were recognized in different microstructural contexts within the sample. Most of these grains can be found in the matrix in close association with biotite, quartz, and plagioclase (Fig. 2a). Monazite was also found as inclusions in garnet and staurolite porphyroblasts (Fig. 2b), and rarely in andalusite. In the case of monazite inclusions in garnet, these crystals are found in their rims (associated to Grt_{2-3}; Fig. 2c). Both Grt_{2-3} and staurolites are linked to the development of the M_3 metamorphic event as well as monazites in the matrix related to S_2 foliation.

The analyzed monazite crystals from the matrix are subhedral with sizes ranging from 28 µm to 64 µm (Fig. 2a). Only one grain was found as an inclusion in an andalusite porphyroblast with lobate borders and a lenght of ~ 24 µm. Monazite crystals that occur as inclusions in staurolite and garnet rims range in size between 20 µm and 60 µm (Fig. 2b).

Monazite dating

Microprobe analyses and compositional X-ray mapping reveals that all the analyzed monazites regarding their context exhibit a marked compositional zoning. Fifty-nine point analyses were obtained from twenty-four monazite grains from different contexts of the same sample. Element X-ray mapping shows that all crystal cores present high Th contents and lower contents of Ce, whereas monazite rims have higher contents of Ce and lower amounts of Th (Fig. 2d). UO_2 contents goes from 0.14 to 0.6 wt.% with scattered values of 0.9 and 1.1 wt%. Contents of ThO_2 and Y_2O_3 do not significantly differ between grains in the matrix and inclusions. For monazites in the matrix ThO_2 varies between 2.11 and 11.5 wt%, whereas ThO_2 in monazite as inclusions range from 2.37 to 13.01 wt%. Moreover, Y_2O_3 content in monazites from the matrix oscillates between 1.01 and 1.46 wt%, while monazites as inclusions range from 1.02 to 1.67 wt%. Also, there is a wide range of Th/U values (between 3.60 and 49.20).

Three main groups of ages can be defined from the analysis of single ages using the unmix routine and weighted average ages from Isoplot (Ludwing 2003). These group of ages are 354 ± 6 Ma (n=15; 2 sigma error), 333 ± 4 Ma (n=33), and 300 ± 11 Ma (n=11) (Fig. 2e). Ages were further determined using the ThO_2*–PbO isochron method proposed by Suzuki and Kato (2008), where regression lines with the coefficient of determination (R^2) are forced through zero (Fig. 2e). The isochrones derived from the defined groups exhibit a strong correlation, each displaying an R^2 value close to 1 (Fig. 2e).

DISCUSSION

P-T-t evolution and regional implications

Maximum sedimentation ages for the protolith of the area were calculated with U-Pb detrital zircon ages at upper Devonian (Hervé et al. 2018). Moreover, the metasedimentary succession from the studied area exhibits two foliations (S_1 and S_2) where the main one is defined as a S_2 crenulation foliation. S_1 is recognized at microscale and can be identified by the alignment of biotite (Bt_1) and muscovite (Ms_1). S_1 can be related to a first deformational event (D_1) and to the first metamorphic event (M_1). This tectono-metamorphic event can be related to the oldest group of ages obtained in monazite cores with mean ages of 354 ± 6 Ma.

Prior to the development of the S_2 foliation a second metamorphic event (M_2) is defined by the static growth of garnet (Grt_1) with andalusite porphyroblasts reaching conditions of about 563 °C and 3.3 kbar (Serra-Varela et al. 2024). These authors assigned this metamorphic event to a heating process related to the igneous intrusions in the area. These granitoids were dated by U-Pb in zircon at 329 ± 4 Ma (Pankhurst et al. 2006). This age is consistent with the

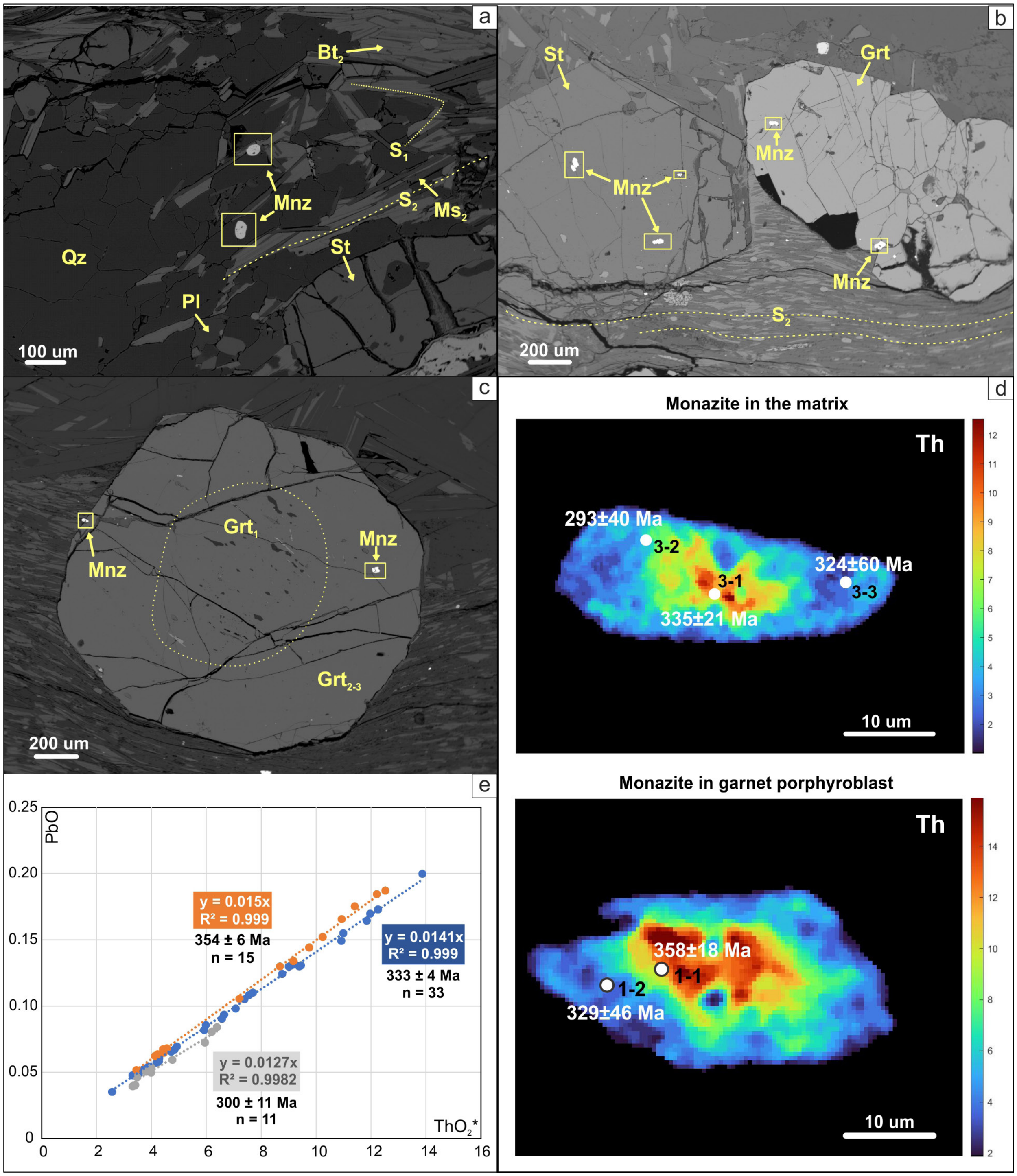

Figure 2. a-b Backscattered electron (BSE) image from the analyzed sample. Monazite crystals in the matrix (a), as inclusions in staurolite and garnet porphyroblasts (b) and in large garnet porphyroblasts where Grt_1 and Grt_{2-3} can be distinguished c. Notice that monazite inclusions are distributed in garnet mantle and rim. d. Compositional X-ray map for Th showing the zoning pattern of the crystals in monazites from different microstructural contexts. Circles indicate the location of the spots and their corresponding age (error at 2σ level). e. Total ThO_2* vs PbO (wt.%) isochrones diagrams weighted average ages (Ma) with MSWD and minimal 2σ error are calculated from single analyses (Ludwing 2003). See the text for further information.

second group of ages determined with a mean age of 333 ± 4 Ma. This igneous event that occurred during the lower Carboniferous would be responsible for the M_2 metamorphic event. Moreover, metamorphic zircon rims in a nearby area, dated by U-Pb SHRIMP, record ages between 330 – 340 Ma (Pankhurst et al. 2006). In addition, 323 ± 5 Ma and 311 ± 27 Ma regional metamorphic ages were obtained south of this region by CHIME method in monazite in paragneises from Paso del

Table 1. Electron probe microanalysis of monazite from andalusite – garnet – sillimanite – staurolite schist (MNP 055).

Spot	ThO_2 (wt%)	Y_2O_3 (wt%)	UO_2 (wt%)	PbO (wt%)	Th (Error%)	Y (Error%)	U (Error%)	Pb (Error%)	Y (ppm)	Th (ppm)	sd (2 sig)	U (ppm)	sd (2 sig)	Pb (ppm)	sd (2 sig)	ThO_2*	Calcula-ted ages	sd (2 sig)
28055-mnz-1-1	9.950	1.022	0.300	0.166	0.270	2.110	2.250	2.580	4021.849	87441.532	472.184	2645.376	119.042	1536.366	79.276	10.931	358	18
28055-mnz-11-1	3.520	1.131	0.216	0.063	0.520	2.010	3.330	6.080	4454.153	30934.090	321.715	1901.391	126.633	588.554	71.568	4.225	355	42
28055-mnz-11-2	5.100	1.113	0.252	0.082	0.410	1.990	2.820	4.920	4382.102	44819.278	367.518	2223.138	125.385	759.364	74.721	5.922	327	32
28055-mnz-11-3	10.030	1.248	0.294	0.155	0.270	1.860	2.300	2.720	4915.199	88144.579	475.981	2593.367	119.295	1437.964	78.225	10.990	333	18
28055-mnz-1-2	3.300	1.039	0.180	0.054	0.540	2.120	3.940	7.060	4089.962	29000.709	313.208	1589.341	125.240	502.220	70.913	3.888	329	46
28055-mnz-12-1	8.570	1.280	0.360	0.144	0.300	1.840	2.000	2.890	5039.615	75313.962	451.884	3172.512	126.900	1336.778	77.266	9.746	349	20
28055-mnz-12-2	4.090	1.350	0.256	0.069	0.470	1.790	2.860	5.560	5315.219	35943.303	337.867	2252.228	128.827	643.324	71.538	4.924	333	36
28055-mnz-12-3	2.850	1.011	0.172	0.040	0.590	2.130	4.030	8.930	3978.540	25046.067	295.544	1517.058	122.275	374.112	66.816	3.409	280	49
28055-mnz-13-1	8.200	1.217	0.287	0.131	0.310	1.910	2.410	3.150	4790.390	72062.368	446.787	2526.374	121.771	1218.881	76.790	9.135	340	21
28055-mnz-13-2	2.740	1.206	0.385	0.053	0.620	1.920	2.050	7.020	4747.868	24079.377	298.584	3396.412	139.253	495.722	69.599	3.995	317	44
28055-mnz-13-3	7.850	1.157	0.254	0.130	0.310	1.930	2.670	3.170	4556.520	68986.535	427.717	2241.650	119.704	1204.957	76.394	8.681	353	22
28055-mnz-13-4	2.150	1.130	0.358	0.048	0.730	2.040	2.200	7.830	4449.822	18894.401	275.858	3158.408	138.970	441.879	69.198	3.320	340	52
28055-mnz-14-1	11.000	1.078	0.257	0.164	0.260	2.020	2.450	2.500	4243.907	96669.030	502.679	2266.332	111.050	1525.226	76.261	11.838	328	16
28055-mnz-14-2	5.770	1.310	0.440	0.105	0.380	1.810	1.770	3.820	5157.731	50707.300	385.375	3878.592	137.302	977.519	74.682	7.207	346	26
28055-mnz-14-3	4.140	1.156	0.216	0.067	0.470	1.990	3.330	5.680	4551.008	36382.708	341.997	1900.510	126.574	622.901	70.762	4.843	328	37
28055-mnz-14-4	2.780	1.380	0.214	0.046	0.620	1.780	3.420	7.770	5433.335	24430.900	302.943	1887.287	129.090	427.955	66.504	3.477	314	48
28055-mnz-14-5	11.500	1.290	0.312	0.187	0.250	1.810	2.140	2.280	5078.987	101063.077	505.315	2746.748	117.561	1736.883	79.202	12.518	353	16
28055-mnz-15-2	8.630	1.232	0.251	0.131	0.300	1.890	2.660	3.140	4851.810	75841.248	455.047	2209.916	117.568	1212.383	76.138	9.447	327	20
28055-mnz-15-3	2.630	1.161	0.235	0.040	0.630	1.940	3.190	8.970	4571.088	23112.686	291.220	2069.757	132.051	369.471	66.283	3.393	278	49
28055-mnz-15-4	3.950	1.610	1.104	0.108	0.480	1.590	0.840	3.690	6338.890	34712.970	333.245	9734.383	163.538	1004.440	74.128	7.554	340	24
28055-mnz-15-5	8.370	1.290	0.262	0.131	0.300	1.840	2.600	3.080	5078.987	73556.344	441.338	2310.406	120.141	1219.810	75.140	9.225	337	20

Table 1. Electron probe microanalysis of monazite from andalusite – garnet – sillimanite – staurolite schist (MNP 055).

28055-mnz-15-6	4.800	1.370	0.567	0.093	0.430	1.790	1.440	4.220	5393.963	42182.849	362.773	4995.450	143.869	867.049	73.179	6.649	333	27
28055-mnz-15-7	3.400	1.256	0.314	0.067	0.540	1.910	2.410	5.650	4945.516	29879.518	322.699	2764.378	133.243	624.758	70.598	4.425	360	40
28055-mnz-16-1	6.330	1.310	0.325	0.105	0.360	1.800	2.250	3.860	5157.731	55628.633	400.526	2868.395	129.078	974.734	75.249	7.392	336	25
28055-mnz-16-2	2.740	1.116	0.245	0.049	0.610	2.020	3.020	7.610	4394.701	24079.377	293.768	2161.433	130.551	453.947	69.091	3.540	327	49
28055-mnz-16-3	5.150	1.234	0.321	0.080	0.410	1.890	2.310	4.920	4859.291	45258.682	371.121	2833.135	130.891	746.368	73.443	6.196	307	30
28055-mnz-17-1	5.330	1.067	0.380	0.090	0.390	2.060	1.910	4.280	4201.385	46840.539	365.356	3347.048	127.857	838.271	71.756	6.568	325	27
28055-mnz-17-4	3.950	1.101	0.236	0.066	0.480	2.000	3.030	5.770	4334.069	34712.970	333.245	2082.980	126.229	608.048	70.169	4.721	328	37
28055-mnz-18-1	3.060	1.213	0.228	0.050	0.570	1.930	3.200	7.170	4774.247	26891.567	306.564	2013.342	128.854	466.944	66.960	3.804	313	44
28055-mnz-18-4	2.930	1.062	0.161	0.052	0.580	2.080	4.360	7.540	4181.699	25749.114	298.690	1415.686	123.448	478.084	72.095	3.455	352	52
28055-mnz-19-2	10.490	1.196	0.281	0.175	0.270	1.930	2.360	2.430	4709.284	92187.102	497.810	2474.365	116.790	1626.413	79.044	11.408	363	17
28055-mnz-19-3	9.210	1.124	0.314	0.152	0.290	1.990	2.220	2.760	4425.412	80938.342	469.442	2770.548	123.012	1411.972	77.941	10.237	351	19
28055-mnz-19-4	3.290	1.216	0.276	0.057	0.540	1.930	2.730	6.630	4786.059	28912.828	312.259	2429.409	132.646	529.141	70.164	4.188	322	42
28055-mnz-2	2.900	1.420	0.421	0.058	0.600	1.750	1.870	6.130	5590.823	25485.472	305.826	3707.581	138.664	539.353	66.125	4.271	322	39
28055-mnz-21-4	5.130	1.100	0.252	0.072	0.410	2.050	2.840	5.310	4329.344	45082.920	369.680	2216.968	125.924	671.174	71.279	5.948	288	30
28055-mnz-21-5	4.420	1.290	0.478	0.086	0.450	1.810	1.660	4.570	5078.987	38843.374	349.590	4215.324	139.949	793.712	72.545	5.981	338	30
28055-mnz-21-7	9.670	1.232	0.383	0.149	0.280	1.850	1.880	2.770	4848.661	84980.865	475.893	3373.493	126.843	1384.122	76.680	10.918	323	18
28055-mnz-21-8	2.370	1.191	0.292	0.039	0.680	1.940	2.620	9.070	4689.991	20827.782	283.258	2577.500	135.061	365.757	66.348	3.320	281	50
28055-mnz-22-4	2.960	1.268	0.270	0.053	0.580	1.860	2.790	6.840	4991.581	26012.757	301.748	2380.926	132.856	491.080	67.180	3.841	326	44
28055-mnz-23-1	13.010	1.174	0.263	0.200	0.230	1.930	2.390	2.140	4620.697	114333.098	525.932	2321.866	110.985	1854.779	79.385	13.870	340	14
28055-mnz-23-3	8.290	1.230	0.336	0.130	0.300	1.860	2.130	3.130	4841.967	72853.296	437.120	2962.715	126.212	1205.885	75.488	9.386	327	20
28055-mnz-24-1	3.430	1.159	0.311	0.065	0.530	2.000	2.420	5.920	4564.788	30143.161	319.518	2743.222	132.772	598.765	70.894	4.446	343	40
28055-mnz-24-3	8.340	1.166	0.230	0.131	0.300	1.940	2.860	3.140	4589.593	73292.701	439.756	2028.327	116.020	1212.383	76.138	9.091	340	21

Table 1. Electron probe microanalysis of monazite from andalusite – garnet – sillimanite – staurolite schist (MNP 055).

28055-mnz-24-4	3.990	1.670	0.946	0.098	0.480	1.540	0.940	4.080	6575.122	35064.494	336.619	8336.327	156.723	909.752	74.236	7.074	329	26
28055-mnz-3-1	7.540	1.266	0.374	0.124	0.320	1.840	1.950	3.200	4984.100	66262.226	424.078	3298.566	128.644	1152.971	73.790	8.761	335	21
28055-mnz-3-2	3.410	1.050	0.179	0.050	0.530	2.110	3.930	7.010	4134.453	29967.399	317.654	1581.408	124.299	459.517	64.424	3.994	293	40
28055-mnz-3-3	2.110	1.120	0.140	0.035	0.740	2.000	5.090	9.460	4409.269	18542.878	274.435	1235.860	125.811	325.840	61.649	2.567	324	60
28055-mnz-4-2	3.410	1.460	0.914	0.084	0.530	1.690	0.970	4.550	5748.310	29967.399	317.654	8052.485	156.218	779.787	70.961	6.385	312	28
28055-mnz-4-3	3.120	1.173	0.506	0.059	0.560	1.940	1.590	6.420	4619.122	27418.852	307.091	4461.262	141.868	549.564	70.564	4.766	295	37
28055-mnz-5-1	11.260	1.270	0.291	0.184	0.260	1.830	2.260	2.370	5000.243	98953.934	514.560	2565.159	115.945	1711.818	81.140	12.211	357	17
28055-mnz-5-2	3.070	1.086	0.190	0.052	0.570	2.060	3.770	7.350	4273.829	26979.447	307.566	1671.320	126.018	479.940	70.551	3.688	332	48
28055-mnz-6-1	11.050	1.184	0.281	0.170	0.260	1.910	2.340	2.490	4662.037	97108.435	504.964	2475.247	115.842	1575.355	78.453	11.966	335	16
28055-mnz-6-2	6.760	1.264	0.286	0.110	0.350	1.850	2.480	3.640	4977.013	59407.513	415.853	2524.611	125.221	1021.150	74.340	7.695	338	24
28055-mnz-7-1	8.250	1.147	0.284	0.134	0.310	1.990	2.440	3.080	4515.573	72501.772	449.511	2499.047	121.953	1243.946	76.627	9.176	345	21
28055-mnz-7-2	3.240	1.088	0.321	0.061	0.550	2.030	2.370	6.370	4282.098	28473.423	313.208	2825.201	133.915	561.632	71.552	4.286	334	42
28055-mnz-8-1	7.910	1.132	0.336	0.130	0.310	2.010	2.120	3.220	4455.728	69513.821	430.986	2961.834	125.582	1204.028	77.539	9.007	340	22
28055-mnz-8-3	3.170	1.065	0.295	0.062	0.550	2.040	2.570	6.210	4193.117	27858.257	306.441	2596.893	133.480	577.414	71.715	4.133	356	43
28055-mnz-9-1	11.310	1.234	0.289	0.173	0.250	1.900	2.280	2.470	4856.535	99393.339	496.967	2546.648	116.127	1605.062	79.290	12.253	334	16
28055-mnz-9-2	3.390	1.243	0.360	0.068	0.530	1.880	2.160	5.750	4893.151	29791.637	315.791	3169.867	136.938	630.328	72.488	4.565	352	40

Sapo and La Potranca area (Renda et al. 2021, Murra et al. 2022, respectively). All these ages are consistent with the development of a magmatic arc associated with metamorphic and deformational events of lower Pennsylvanian age, which different authors relate to an active subduction zone (Pankhurst et al. 2006, Heredia et al. 2016, Hervé et al. 2018, Renda et al. 2021, Rapela et al. 2024, and references therin). Finally, a main tectono-metamorphic event (M_3) is recognized in the sample with the development of a penetrative S_2 foliation and a mineral assemblage of garnet (Grt_{2-3}), sillimanite, staurolite, biotite (Bt_2), muscovite (Ms_2), plagioclase, and quartz. For this event, Serra-Varela et al. (2024) calculated an increase in pressure and temperature from conditions similar to M_2 up to 5.6 - 6.6 kbar and 630-650 °C which represents main peak metamorphic conditions for this unit.

Furthermore, the lower Carboniferous igneous rocks exhibit deformation marked by the development of a metamorphic foliation. This deformation corresponds to the M_3 event associated with the S_2 foliation. The M_3 event has been constrained to approximately 300 Ma based on monazite ages from a mica schist sample (this study). Regionally, this event is also identified in metamorphic rocks of the North Patagonian Cordillera and the extra-Andean region, where monazite ages range between approximately 311 and 299 Ma (Oriolo et al. 2019).

CONCLUSION

The complex polymetamorphic history of the andalusite-garnet-staurolite-sillimanite schist from the Cushamen Complex, highlights the importance of dating methods of minerals that preserve the metamorphic history, as this information becomes critical for a meaningful interpretation of the ages.

X-ray elemental distribution maps show that, regardless of the microstructural context, all monazites exhibit zoning, with Th depletion and Ce enrichment towards the rims. Three groups of ages were determined from all monazite analyses taking into account their chemical variations from the recognized zoning patterns (354 ± 6 Ma, 333 ± 4 Ma, and 300 ± 11 Ma) that correlate with the previously described M_1, M_2, and M_3 events for this rock. It should be noted that all monazites regarding the microstructural domain in which they were analyzed show the same chemical zoning. On a wider scale, the results are within the age range established for metamorphic events identified regionally in North Patagonia, giving further support to our findings. This study represents the first published CHIME monazite age obtained in a lab located in Argentina, marking a historic milestone for metamorphic petrology and opening new possibilities for petrochronological research in the country.

ACKNOWLEDGEMENTS

This work has been supported by projects PICT-2017-0619, PICT-2020-SERIEA-01937 and SECyT UNC 2023–2027. We would also like to thank LAMARX operators and technicians for their good predisposition in setting up the CHIME technique. We would like to thank Dr. Eber Cristofolini and Dr. Sebastián Oriolo for their comments that helped to improve the manuscript as well as Dra. Alina Tibaldi for her comments and diligent editorial handling of the manuscript.

REFERENCES

Cerredo, M.E. 1997. The metamorphism of Cushamen Formation, Río Chico area. North Patagonian Massif, Argentina. In: VIII Congreso Geológico Chileno 2: 1236–1240. Antofagasta.

Cerredo, M.E., and López De Luchi, M.G. 1998. Mamil choique granitoids, southwestern North Patagonian Massif, Argentina: Magmatism and metamorphism associated with a polyphasic evolution. Journal of South American Earth Sciences 11: 499–515.

Dalla Salda, L.H., Varela, R., Cingolani, C., and Aragón, E. 1994. The Río Chico Paleozoic crystalline complex and the evolution of northern Patagonia. Journal of South American Earth Sciences 7: 377–386.

Dicaro, S., González, S.N., Serra-Varela, S., and Heredia, N. 2023. Structure and metamorphism of the Cushamen Complex in Sañicó and Collón Curá-Limay rivers confluence: a Devonian metamorphic event related to the subduction stage of the Gondwanan Patagonian orogen. Journal of South American Earth Sciences 121: 104–152.

Duhart, P., Haller, M., and Hervé, F. 2002. Diamictitas como parte del protolito de las metamorfitas de la Formación Cushamen en Río Chico, Provincias de Río Negro y Chubut, Argentina. In: XV Congreso Geológico Argentino 2: 97–100.

Engi, M., Lanari, P., and Kohn, M.J. 2017. Significant ages-An introduction to petrochronology. Reviews in Mineralogy and Geochemistry 83(1): 1–12.

Falco, J. I., Hauser, N., Scivetti, N., Reimold, W. U., and Folguera, A. 2022. The origin of Patagonia: insights from Permian to Middle Triassic magmatism of the North Patagonian Massif. Geological Magazine 159(9): 1490-1512.

García-Sansegundo, J., Farias, P., Gallastegui, G., Giacosa, R.E., and Heredia, N. 2009. Structure and metamorphism of the Gondwanan basement in the Bariloche region (North Patagonian Argentine Andes). International Journal of Earth Sciences 98: 1599–1608.

Giacosa, R., Márquez, M., Nillni, A., Fernández, M., Fracchia, D., Parisi, C., Afonso, J., Paredes, J., and Sciutto, J. 2004. Litología y estructura del basamento ígneo-metamórfico del borde SO del Macizo Nordpatagónico al oeste del Río Chico (Cushamen, Chubut, 42° 10´ S-70° 30´ O). Revista de la Asociación Geológica Argentina 59(4): 569–577

Heredia, N., García-Sansegundo, J., Gallastegui, G., Farias, P., Giacosa, R., Alonso, J.L., Busquets, P., Charrier, R., Clariana, P., Colombo, F., Cuesta, A., Gallastegui, J., Giambiagi, L., González-Menéndez, L., Limarino, C.O., Martín-González, F., Méndez Bedia, I., Pedreira, D., Quintana, L., Rodríguez-Fernández, L.R., Rubio-Ordonez, A., Seggiaro, R., Serra-Varela, S., Spalletti, L., Cardo, R., and Ramos V.A. 2016. Evolución Geodinámica de los Andes argentino-chilenos y la Península Antártica durante el Neoproterozoico tardío y el Paleozoico. Trabajos de Geología, Universidad de Oviedo 36: 237–278.

Heredia, N., García-Sansegundo, J., Gallastegui, G., Farias, P., Giacosa, R., Hongn, F., Tubía, J.M., Alonso, J.J., Busquets, P., Charrier, R., Clariana, P., Colombo, F., Cuesta, A., Gallastegui, J., Giambiagi, L., González Menéndez, L., Limarino, O., Martín-González, F., Pedreira, D., Quintana, L., Rodríguez-Fernández, L.R., Rubio-Ordóñez, Á., Seggiaro, R., Serra-Varela, S., Spalletti, L., Cardó, R., and Ramos, V.A. 2018. The preandean phases of construction of the southern andes basement in neoproterozoic–paleozoic times. In: Folguera, A., Contreras Reyes, E., Heredia, N., Encinas, A., Oliveros, V., Dávila, F., Collo, G., Giambiagi, L., Maksymowicz, A., Iglesia Llanos, M.P., Turienzo, M., Naipauer, M., Orts, D., Litvak, V., Alvarez, O., and Arriagada, C. (Eds.). The evolution of the Chilean Argentinean Andes, Switzerland, Springer-Verlag111–131.

Hervé, F., Calderón, M., Fanning, C.M., Pankhurst, R.J., Rapela, C.W., and Quezada, P. 2018. The country rocks of Devonian magmatism in the North Patagonian Massif and Chaitenia. Andean Geology 45: 301–317.

López de Luchi, M.G., Rapalini, A.E., and Tomezzoli, R.N. 2010. Magnetic fabric and microstructures of Late Paleozoic granitoids from the North Patagonian Massif: Evidence of a collision between Patagonia and Gondwana?. Tectonophysics 494(1–2): 118–137.

Lucassen, F., Trumbull, R., Franz, G., Creixell, C., Vásquez, P., Romer, R.L., and Figueroa, O. 2004. Distinguishing crustal recycling and juvenile additions at active continental margins: the Paleozoic to recent compositional evolution of the Chilean Pacific margin (36–41°S). Journal of South American Earth Sciences 17: 103–119.

Ludwig, K.R. 2003. User's manual for isoplot 3.00, a geochronlogical toolkit for microsoft excel. Berkeley Geochronology Center Special. Publication 4: 25–32.

Marcos, P., Pavón Pivetta, C., Benedini, L., Gregori, D.A., Geraldes, M.C., Scivetti, N., Barros, M., Varela, M.E., and Dos Santos A. 2020. Late Paleozoic geodynamic evolution of the western North Patagonian Massif and its tectonic context along the southwestern Gondwana margin. Lithos 376–377: 105801.

Marcos, P., Renda, E., González, P. D., Oriolo, S., Scivetti, N., Benedini, L., Geraldes, M., Gregori, D., Yoya, M., and Bahia, M. 2023. Devonian to early Carboniferous advancing-retreating subduction switch in southern South America: U-Pb and Lu-Hf isotopic insights. Tectonics 42(11): e2022TC007533.

Martínez, J.C., Dristas, J.A., and Massonne H.J. 2012. Palaeozoic accretion of the microcontinent Chilenia, North Patagonian Andes: high pressure metamorphism and subsequent thermal relaxation. International Geology Review 54(4): 472–490.

Murra, J.A., Baldo, E.G., Verdecchia, S.O., Ramacciotti, C.D., and Galindo C. 2022. El Escorial calcitic marbles (Cushamen Metamorphic Complex, Macizo Norpatagónico): $^{87}Sr/^{86}Sr$ isotopic characterization and age of sedimentation. Andean Geology 49(1): 77–93.

Oriolo, S., Schulz, B., González, P.D., Bechis, F., Olaizola, E., Krause, J., Renda, E.M., and Vizán, H. 2019. The Late Paleozoic tectonometamorphic evolution of Patagonia revisited: Insights from the pressure-temperature-deformation-time (P-T-D-t) path of the Gondwanide basement of the North Patagonian Cordillera (Argentina). Tectonics 38(7): 2378–2400.

Pankhurst, R.J., Rapela, C.W., Fanning, C.M., and Márquez, M. 2006. Gondwanide continental collision and the origin of Patagonia. Earth Science Review 76(3–4): 235–257.

Rapela, C.W., García, M., Hervé, F., Pankhurst, R.J., Calderon, M., Fanning, C.M., and Verdecchia, S.O. 2024. Late Paleozoic magmatism and foreland deformation associated with opening and closing of marginal basins in the North Patagonian Andes. Journal of the Geological Society 181(2): 1–18.

Renda, E. M., González, P. D., Vizán, H., Oriolo, S., Prezzi, C., González, V. R., Schulz, B., Krause, J., and Basei, M. 2021. Igneous-metamorphic basement of Taquetrén Range, patagonia, Argentina: A key locality for the reconstruction of the paleozoic evolution of Patagonia. Journal of South American Earth Sciences 106: 103045.

Serra-Varela, S., Heredia, N., Giacosa, R., García-Sansegundo, J., and Farias, P. 2020. Review of the polyorogenic Palaeozoic basement of the Argentinean North Patagonian Andes: age, correlations, tectonostratigraphic interpretation and geodynamic evolution. International Geology Review 64(1): 72–95.

Serra-Varela, S., Verdecchia, S.O, Lembo Wuest, C.I., Benítez, M.E, Murra, J., and Baldo, E.G. 2024. Polymetamorphic P–T evolution of the andalusite–garnet–staurolite–sillimanite-bearingschist from the Cushamen Complex (Argentina). International Journal of Earth Sciences (Geol Rundsch) 113: 1385–1406.

Suzuki, K., and Kato, T. 2008. CHIME dating of monazite, xenotime, zircon and polycrase: Protocol, pitfalls and chemical criterion of possibly discordant age data. Gondwana Research 14(4): 569–586.

Varela, R., Basei, M.A.S., Cingolani, C.A., and Passarelli, C.R. 2005. El basamento cristalino de los Andes norpatagónicos en Argentina: Geocronología e interpretación tectónica. Revista Geológica de Chile 32: 167–187.

Varela, R., Gregori, D.A., González, P.D., and Basei, M.A. 2015. Caracterización geoquímica del magmatismo de arco devónico y carbonífero-pérmico en el noroeste de Patagonia, Argentina. Revista de la Asociación Geológica Argentina 72(3): 419–432.

Vlach, S.R.F. 2010. Th-U-PbT dating by Electron Probe Microanalysis, Part I. Monazite: analytical procedures and data treatment. Geologia USP, Série Científica 10(1): 61–85.

Volkheimer, W. 1964. Estratigrafía de la zona extrandina del Departamento de Cushamen (Chubut) entre los paralelos 42° y 42° 30’ y los meridianos 70° y 71°. Revista de la Asociación Geológica Argentina 19(2): 85–107.

Whitney, D.L., and Evans, B.W. 2010. Abbreviations for names of rock-forming minerals. American Mineralogist 95:185–187.

Williams, M.L., Jercinovic, M.J., Mahan, K.H., and Dumond, G. 2017. Electron microprobe petrochronology. Reviews in Mineralogy and Geochemistry 83(1): 153–182.